

# Generation of a microresonator soliton comb pumped by a DFB laser with phase noise measurements

KENJI NISHIMOTO,<sup>1</sup> KAORU MINOSHIMA,<sup>2,3</sup> TAKESHI YASUI,<sup>3,4</sup> AND NAOYA KUSE<sup>3,5,\*</sup>

<sup>1</sup>*Faculty of Science and Technology, Tokushima University, 2-1, Minami-Josanjima, Tokushima, Tokushima 770-8506, Japan*

<sup>2</sup>*Graduate School of Informatics and Engineering, The University of Electro-Communications, 1-5-1 Chofugaoka, Chofu, Tokyo 182-8585, Japan*

<sup>3</sup>*Institute of Post-LED Photonics, Tokushima University, 2-1, Minami-Josanjima, Tokushima, Tokushima 770-8506, Japan*

<sup>4</sup>*Graduate School of Technology, Industrial and Social Sciences, Tokushima University, 2-1, Minami-Josanjima, Tokushima, Tokushima 770-8506, Japan*

<sup>5</sup>*PRESTO, Japan Science and Technology Agency, 4-1-8 Honcho, Kawaguchi, Saitama, 332-0012, Japan*

\**kuse.naoya@tokushima-u.ac.jp*

**Abstract:** Optical frequency combs generated from microresonators have the potential to be fully chip-scale optical frequency combs. In conjunction with the recent advances in fabrication techniques of high-Q microresonators, there has been progress in the minimization of systems for the generation of microresonator soliton combs. This progress is highlighted by the co-integration of a pump continuous-wave (cw) laser with a microresonator, in which self-injection locking is utilized. Although the use of self-injection locking overcomes the fast thermal dynamics of microresonators, the technique does not allow the simultaneous operation of multiple soliton combs by one pump laser. Here, we demonstrate the generation of a soliton comb by a compact cw laser (distributed feedback (DFB) laser) without self-injection locking. Because of the fast scan speed of the DFB laser, a single soliton comb is generated simply by controlling the injection current of the DFB laser, even if soliton steps have a short lifetime of  $< 100$  ns. In addition, we measured the influence of the phase noise of the DFB laser on the phase noise of the soliton comb mode and the timing jitter of the soliton comb, and compared with those of the soliton comb generated from a low noise cw laser.

© 2021 Optical Society of America under the terms of the [OSA Open Access Publishing Agreement](#)

## 1. Introduction

Recent advances in fabricating high-Q microresonators have enabled the minimization of optical frequency combs, to the potentially chip-scale, highlighted as microcombs [1, 2]. In particular, dissipative Kerr microresonator soliton combs (hereafter called soliton combs), which is a mode-locked state, produce highly coherent optical frequency combs with ultra-short pulse trains [3]. The comb mode spacing of the soliton combs ranges from tens of GHz to THz, allowing easy access to each comb mode. Large comb mode spacing has been utilized in applications such as coherent optical communication [4], ultra-fast ranging [5, 6], THz-wave generation [7], and astrophysical spectrometer calibration [8, 9].

Among the various platforms utilized to generate soliton combs, Si<sub>3</sub>N<sub>4</sub> (SiN) [10–12], AlN [13], and LiNbO<sub>3</sub> [14, 15] have been promising for mass manufacturing because of the CMOS compatible fabrication process. Very recently, high-Q microresonators made of III-V materials such as GaP [16] and AlGaAs [17], have also been demonstrated, potentially providing the integration of both the microresonator and pump continuous-wave (cw) laser onto one chip. With the development of microresonators based on SiN with  $Q > 10^7$  [18–20], which requires

< 100 mW pump power for the generation of soliton combs, chip-scale soliton combs have been generated by butt-coupling a pump cw laser to a microresonator without having optical amplifiers [21–25]. In these reports, Rayleigh back-scattering from a microresonator is injected into a pump cw laser, enforcing the oscillation frequency of the pump cw laser to be equal (or with offset in some cases) to the resonance frequency of the microresonator, when the resonance frequency is within the injection locking range of the pump cw laser. The self-injection locking method has two advantages. First, the use of an optical isolator between the pump cw laser and microresonator can be avoided. Second, the fast thermal dynamics of the microresonator, which discontinues the soliton states in a short time (e.g. < 100 ns for some microresonators based on SiN) after the transition from the chaotic to the soliton regime, can be overcome because of the fast dynamics of self-injection locking, avoiding the conventional requirements of fast tuning of the pump frequency by a carrier-suppressed single-sideband modulator (CS-SSB modulator) [12], fast tuning of the resonance frequency by an integrated microheater [11] and pump power modulation [10], and the utilization of an auxiliary cw laser [26–28]. However, a recent theoretical and experimental demonstration of self-injection locking shows that the dynamics of self-injection locking is sensitive to various parameters, e.g., strength and phase of the backscattering and pump power [24]. In particular, phase adjustment is crucial for accessing a single soliton state, which may hinder the reliable operation of the soliton combs in practical situations. In addition, it is very likely difficult for self-injection locking to operate several soliton combs with one pump cw laser as demonstrated in tandem [29], parallel [30], and bidirectional configurations [31,32], disabling simple dual-comb systems with mutual coherence for dual-comb ranging [5,6], dual-comb spectroscopy [29,33,34], dual-comb imaging [35] and dual-comb spectrometry [36]. Thus, the generation of soliton combs without self-injection locking remains necessary.

Conventionally, without self-injection locking, soliton combs are generated with pump cw lasers based on either a bulky external cavity diode laser (ECDL) (e.g, CTL 1550, Toptica Photonics) [3, 12–17, 26, 27, 31–33, 35, 36] or a planar waveguide external cavity laser (PW-ECL) (e.g, RIO, RIO-Optasense Inc.) [11, 29, 30]. To realize a compact soliton comb system, the bulky ECDL cannot be used. Although PW-ECL can be compact and has a narrow linewidth (< 10 kHz), the tuning range and speed of the optical frequency are quite limited for the generation of soliton combs, e.g., < 200 MHz in 0.1 ms for RIO. Therefore, PW-ECL requires either an integrated microheater on microresonators or a CS-SSB modulator. Furthermore, such a narrow scan range does not allow soliton-comb-based high-resolution spectroscopy [30,37,38], recently demonstrated massively parallel coherent LIDAR [39], and frequency-modulated comb LIDAR [40]. Another compact pump cw laser is a distributed feedback cw (DFB) laser. At the expense of the moderately broad linewidth (< 1 MHz) of DFB lasers, their scan range (> 200 GHz) and speed (100 THz/s or even faster in the adiabatic case) are very attractive for the applications mentioned above, which do not necessarily require a narrow linewidth pump cw laser. However, there has been no demonstration, to the best of our knowledge, of the generation of soliton combs from DFB lasers without self-injection locking.

In this letter, we present the generation of a single soliton comb with the use of a DFB laser. Owing to the fast scan speed of the DFB laser, a single soliton comb can be generated by simply modulating the injection current of the DFB laser. In addition, we measured the phase noise of the soliton comb mode and the timing jitter of the soliton comb, compared with the soliton comb generated from a bulky ECDL (the linewidth of < 10 kHz). Because the phase noise of the soliton comb mode and timing jitter of the soliton comb generated from the bulky ECDL are limited by the thermo-reflective noise of the microresonator, the drawback of the DFB laser, i.e., moderately broad linewidth, is not very critical. In fact, only a slight difference between the bulky ECDL and the DFB laser is realized when a cutting-edge DFB laser [24] is used, while the advantages of fast scan speed and large scan range are maintained.

## 2. Results

### 2.1. Experimental setup

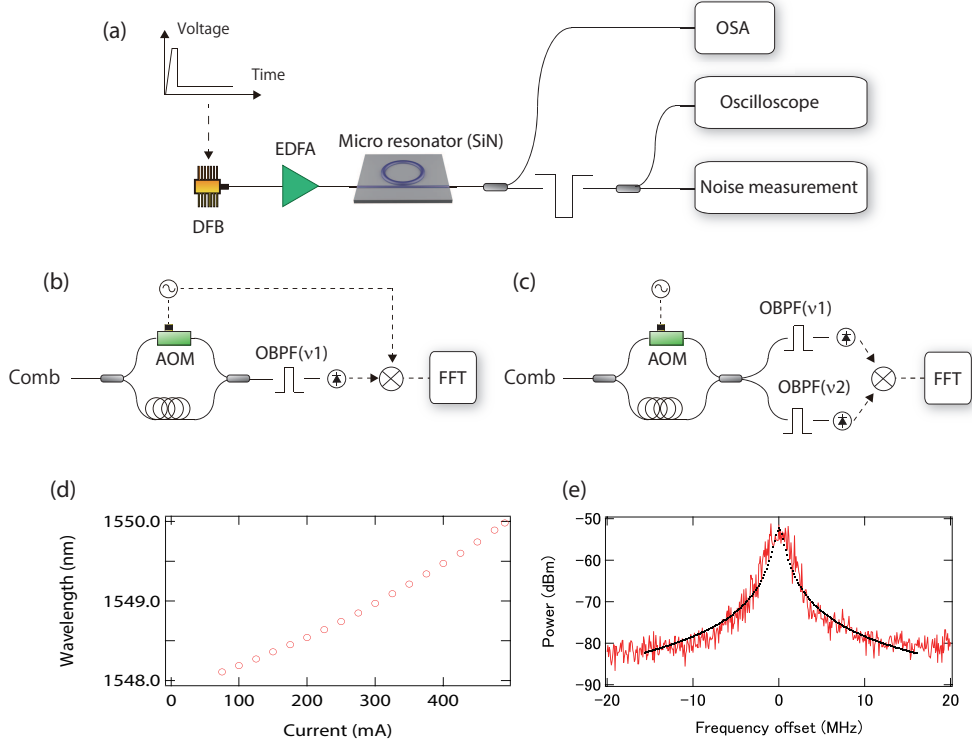


Fig. 1. (a) Schematic of the experimental setup to generate a soliton comb. DFB: distributed feedback laser, EDFA: Er-doped fiber amplifier, OSA: optical spectral analyzer. (b) Schematic of the experimental setup to measure the phase noise of the soliton comb mode. AOM: acousto-optic modulator, OBPF: optical bandpass filter. (c) Schematic of the experimental setup to measure the timing jitter of the soliton comb. (d) Tuning range of the DFB laser wavelength. (e) RF spectrum of a beat between the DFB laser and an optical fiber frequency comb. Dotted black curve shows the fitted Lorentz function with an FWHM of 1 MHz.

The experimental setup is shown in Fig. 1(a). A DFB laser oscillating near 1548 nm was used as the pump cw laser. The output from the DFB laser is amplified by an Er-doped fiber amplifier (EDFA) with one forward and two backward pump laser diodes (LDs). The maximum output from the EDFA is approximately 500 mW. The output from the EDFA is coupled into a high-Q microresonator based on SiN through a lensed fiber. The free spectral range (FSR) and Q of the microresonator are approximately 540 GHz and  $10^6$ , respectively. The output from the microresonator is split into two outputs. One is used to measure the optical spectrum of the generated soliton comb. The other is directed to a bandstop filter to reject the residual of the DFB laser, followed by a  $1 \times 2$  splitter. To measure the time evolution of the power of the generated comb, one of the two outputs from the bandstop filter is monitored by an oscilloscope, whereas the other output is used to measure the phase noise of the soliton comb modes ( $L_{\text{mode,DFB}}(f)$ ) and timing jitter of the soliton comb ( $L_{\text{jitter,DFB}}(f)$ ). The wavelength of the DFB laser is scanned by changing the injection current through an arbitrary frequency generator to generate a single soliton comb. The details are shown in the next section. Figures 1(b) and

(c) show the experimental designs used to measure  $L_{\text{mode,DFB}}(f)$  and  $L_{\text{jitter,DFB}}(f)$ , respectively.  $L_{\text{mode,DFB}}(f)$  is measured by a delayed self-heterodyne interferometer, which consists of an imbalanced Mach-Zehnder interferometer (MZI) with an acousto-optic modulator (AOM) in one arm of the MZI. An optical bandpass filter is installed before photo detection to leave only one comb mode. For the measurement of  $L_{\text{jitter,DFB}}(f)$ , a two-wavelength delayed self-heterodyne interferometer (TWDI) [41–43] is used. The TWDI uses two outputs from an imbalanced MZI. Each output passes an optical bandpass filter, both of which pass through two comb modes at different wavelengths. By mixing the photo-detected signals, the quantity  $N^2 \times L_{\text{jitter,DFB}}(f)$ , where  $N$  is the separation of the comb mode number between the two outputs from the optical bandpass filters, can be measured after calibration, while the carrier envelope offset frequency of the soliton comb is cancelled. Details of the TWDI are shown in ref [42, 43].

Figure 1(d) shows the tuning range of the wavelength of the DFB laser when the injection current is changed. The tuning range is approximately 2 nm (250 GHz) without mode-hopping. This tuning range is sufficiently large to cover one FSR of most of the soliton comb when the DFB laser is used for comb mode scanning [30, 38]. The linewidth of the DFB laser is also measured by taking a beat between an optical fiber frequency comb and the DFB laser (Fig. 1(e)), which shows an FWHM of approximately 1 MHz.

### 2.1.1. Soliton comb generation

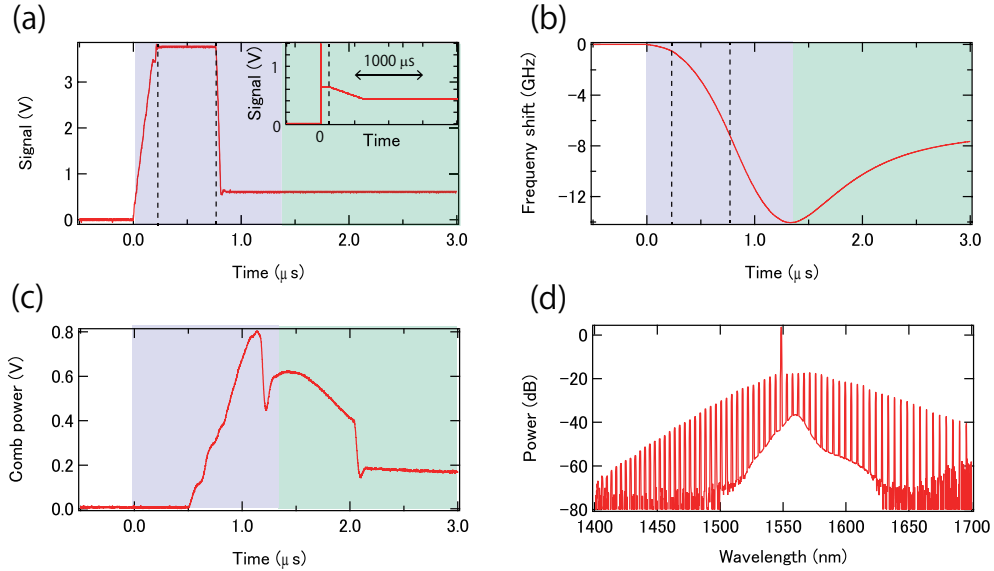


Fig. 2. (a) Control signal for the injection current of the DFB laser. The inset shows the control signal with a long time span. (b) Change in frequency of the DFB laser with the control signal. (c) Time evolution of the comb power when the frequency of the DFB laser is scanned. The blue/green area shows the time when the frequency of the DFB laser is decreasing/increasing. (d) Optical spectrum of a soliton comb.

To generate a soliton comb, the fast thermal dynamics of the microresonator must be addressed. One novel method is to utilize self-injection locking, as explained in the introduction. Without self-injection locking, either (or both) the frequency of the pump cw laser or the resonance frequency of the microresonator must be rapidly controlled. Rapid control has been demonstrated by CS-SSB [12], pump-power kicking [10], an auxiliary cooling laser [7, 26, 28], and integrated microheater [11]. Instead of using these methods, we simply modulate the in-

jection current of the DFB laser. Figures 2(a) and (b) show the control signal of the injection current and frequency change of the DFB laser, respectively. The injection current is increased from  $t = 0$  to 200 ns, decreasing the frequency of the DFB laser adiabatically. From 200 ns to 750 ns, the injection current remains the same; however, the frequency continues to decrease, owing to the delayed thermal response of the DFB laser. At 750 ns, the injection current is rapidly and significantly decreased, causing an increase in the frequency with a slight delay (250 ns). A soliton step is observed between  $1.2 \mu\text{s}$  and  $1.3 \mu\text{s}$  (Fig. 2(c)), showing the increase of the comb power. The increase of the comb power is caused by the increase of the resonance frequency, increasing the detuning. If the optical frequency of the DFB laser starts to increase during the soliton step, a long lifetime ( $> 100 \mu\text{s}$ ) soliton comb with a transition to the single soliton state can be observed (Fig. 2(c)) by following the increase of the resonance frequency. Owing to the slow thermal response of the microresonator, the frequency of the DFB laser needs to be slightly increased at  $140 \mu\text{s}$  (inset in Fig. 2(a)). Then, the single soliton comb is maintained for a few hours without any feedback loops to maintain the detuning. The optical spectrum of the soliton comb is shown in Fig. 2(d). The comb spacing corresponds to the FSR of the microresonator with a  $\text{sech}^2$  envelope, indicating that the soliton comb is a single soliton.

### 2.1.2. Noise measurements

The phase noise of the soliton comb mode and timing jitter of the soliton comb are measured. For comparison, a soliton comb is generated from an ECDL. When the ECDL is used, a CS-SSB as a rapid frequency shifter is inserted between the ECDL and EDFA to generate the soliton comb, since the scan speed of the ECDL is not fast enough to access a stable soliton comb. Figure 3(a) shows the phase noise of the DFB laser ( $L_{\text{DFB}}(f)$ ) and ECDL ( $L_{\text{ECDL}}(f)$ ), which were measured by the same setup as Fig. 1(b).  $L_{\text{DFB}}(f)$  is more than 40 dB worse than  $L_{\text{ECDL}}(f)$  for a frequency offset of 1 kHz to 1 MHz when the acoustic noise between 1 kHz and 10 kHz is neglected. Figure 3(b) shows the phase noise of the soliton comb mode generated by the DFB laser ( $L_{\text{mode,DFB}}(f)$ ) and ECDL ( $L_{\text{mode,ECDL}}(f)$ ).  $L_{\text{mode,DFB}}(f)$  corresponds to  $L_{\text{DFB}}(f)$  as shown in the inset of Fig. 3(b), indicating that the phase noise of the DFB laser is transferred to the comb mode, which is different from the case for the ECDL.  $L_{\text{mode,ECDL}}(f)$  is worse than  $L_{\text{ECDL}}(f)$  by approximately 10 dB at the wide range of the frequency offset. Similar phenomena have been recently observed for the carrier envelope offset frequency [44] and pump cw laser [45], concluding that the increase is caused by the thermo-reflective noise of the microresonator. Because of the thermo-reflective noise, the difference between  $L_{\text{mode,DFB}}(f)$  and  $L_{\text{mode,ECDL}}(f)$  is less than the difference between  $L_{\text{DFB}}(f)$  and  $L_{\text{ECDL}}(f)$ . Meanwhile, the timing jitter of the soliton combs is also measured ( $L_{\text{jitter,DFB}}(f)$  and  $L_{\text{jitter,ECDL}}(f)$  for the soliton combs generated from the DFB laser and the ECDL, respectively). To measure the timing jitter, the comb modes at 1526 and 1535 nm were used in the TWDI. Figure 3(c) shows  $L_{\text{jitter,DFB}}(f)$  and  $L_{\text{jitter,ECDL}}(f)$ , which are scaled to the comb mode spacing (540 GHz in this experiment). The difference between the soliton combs from the DFB laser and the ECDL is even smaller than the difference between  $L_{\text{mode,DFB}}(f)$  and  $L_{\text{mode,ECDL}}(f)$ . For a frequency offset from 100 Hz to 1 kHz,  $L_{\text{jitter,DFB}}(f)$  is almost the same as  $L_{\text{jitter,ECDL}}(f)$ . Above a frequency offset of a few kHz,  $L_{\text{jitter,ECDL}}(f)$  gradually deviates from  $L_{\text{jitter,DFB}}(f)$ . Figure 3(d) shows  $L_{\text{mode,DFB/ECDL}}(f) - L_{\text{jitter,DFB/ECDL}}(f)$ , defined as  $L_{\text{corr,DFB/ECDL}}(f)$ , which is an indicator of the strength of the correlation between the comb modes. For the soliton comb generated from the DFB laser, in which  $L_{\text{jitter,DFB}}(f)$  is limited by  $L_{\text{DFB}}(f)$ ,  $L_{\text{corr,DFB}}(f)$  is approximately 30 dB. Meanwhile, when  $L_{\text{jitter,ECDL}}(f)$  is limited by  $L_{\text{mode,ECDL}}(f)$  (i.e., the thermo-reflective noise limited),  $L_{\text{corr,ECDL}}(f)$  is smaller than  $L_{\text{corr,DFB}}(f)$ , suggesting that thermo-reflective noise is not highly correlated between comb modes. Although the reason is not yet clear, the thermo-reflective noise may be dispersive because of wavelength-dependent effective mode volume in microresonators. The thermo-reflective noise depends on the FSR of the microresonators. In theory, the thermo-reflective noise is inversely proportional

to FSR when a homogeneous microresonator in an infinite heat bath is assumed [46]. However, a numerical simulation shows that the dependency is less than the ideal case [45], which means that the phase noise of DFB lasers is not significantly larger than the thermo-reflective noise even for microresonators with small FSRs.

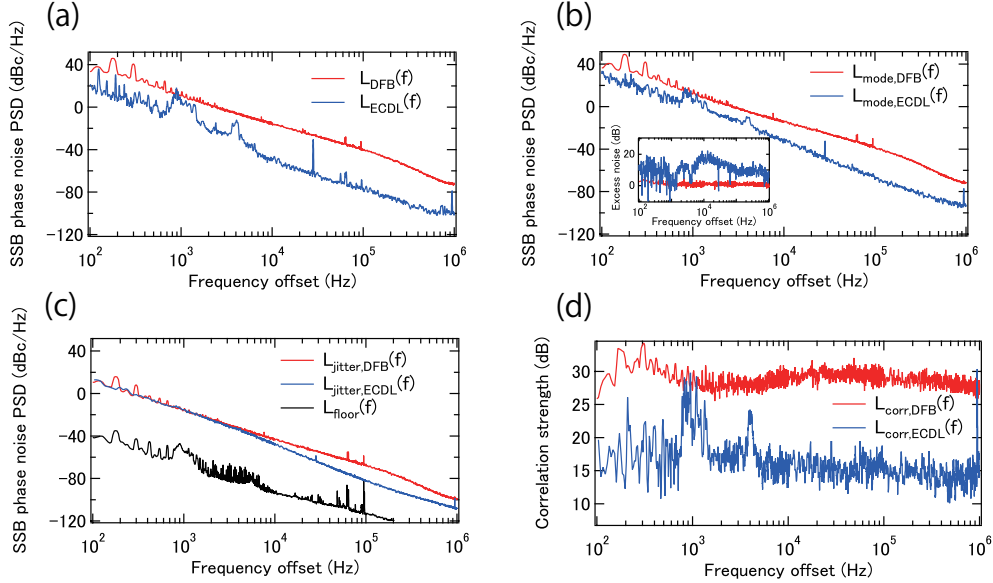


Fig. 3. (a) Single sideband (SSB) phase noise power spectrum density (PSD) of the DFB laser (red) and ECDL (blue). (b) SSB phase noise PSD of the soliton comb mode generated from the DFB laser (red) and ECDL (blue). The inset shows the excess noise compared with the pump cw lasers, that is,  $L_{\text{mode,DFB}}(f) \hat{\sim} L_{\text{DFB}}(f)$  (red) and  $L_{\text{mode,ECDL}}(f) \hat{\sim} L_{\text{ECDL}}(f)$  (blue). (c) SSB phase noise PSD of the timing jitter of the soliton comb generated from the DFB laser (red) and ECDL (blue). The black curve shows the measurement noise floor. (d) Correlation strength between the timing jitter and the comb mode defined as  $L_{\text{mode,DFB}}(f) \hat{\sim} L_{\text{jitter,DFB}}(f)$  (red) and  $L_{\text{mode,ECDL}}(f) \hat{\sim} L_{\text{jitter,ECDL}}(f)$  (blue).

### 3. Conclusion

In conclusion, we demonstrated the generation of a single soliton comb from a DFB laser without self-injection locking, in which only the tuning of the injection current is employed without requiring CS-SSB, power kicking and an auxiliary cooling laser. The phase noise of the comb mode and timing jitter of the soliton comb were also measured and compared with those of the soliton comb generated from an ECDL. We found that the DFB laser has a larger phase noise than the thermo-reflective noise of the microresonator, transferring the phase noise to the soliton comb mode and timing jitter. However, as the thermo-reflective noise of the microresonator was not highly correlated across the soliton comb modes, the timing jitter of the soliton combs generated from the DFB laser was within 20 dB of the soliton combs generated from the ECDL, while the DFB laser maintains the benefits of a large scan range and fast scan speed. In addition, when low noise DFB lasers are used, the phase noise of the low noise DFB lasers can be comparable with the thermo-reflective noise of the microresonator. As mentioned in the introduction, although the generation of soliton combs without self-injection locking is very useful for dual-comb techniques with one pump cw laser, an optical isolator is required. Various studies to integrate optical isolators into photonic circuits, using spatiotemporal modulation of the reflective index [47], nonlinear effects [48], and magneto-optical materials [49] are in

progress [50]. Once integrated optical isolators are realized, chip-scale soliton comb systems without self-injection locking could also be generated through the capability of dual-comb techniques and reproducible operation.

## Funding

This work was financially supported by JST PRESTO (JPMJPR1905), Japan Society for the Promotion of Science (19H00871), Cabinet Office, Government of Japan (Subsidy for Reg. Univ. and Reg. Ind. Creation), and Nakatani Foundation for Advancement of Measuring Technologies in Biomedical Engineering.

## Disclosures

The authors declare no conflicts of interest.

## References

1. T. J. Kippenberg, A. L. Gaeta, M. Lipson, and M. L. Gorodetsky, "Dissipative Kerr solitons in optical microresonators," *Science* **361**, eaan8083 (2018).
2. A. L. Gaeta, M. Lipson, and T. J. Kippenberg, "Photonic-chip-based frequency combs," *Nat. Photonics* **13**, 158 (2019).
3. T. Herr, V. Brasch, J. D. Jost, C. Y. Wang, N. M. Kondratiev, M. L. Gorodetsky, and T. J. Kippenberg, "Temporal solitons in optical microresonators," *Nat. Photonics* **8**, 145–152 (2014).
4. P. Marin-Palomo, J. N. Kemal, M. Karpov, A. Kordts, J. Pfeifle, M. H. P. Pfeiffer, P. Trocha, S. Wolf, V. Brasch, M. H. Anderson, R. Rosenberger, K. Vijayan, W. Freude, T. J. Kippenberg, and C. Koos, "Microresonator-based solitons for massively parallel coherent optical communications," *Nature* **546**, 274–279 (2017).
5. P. Trocha, M. Karpov, D. Ganin, M. H. P. Pfeiffer, A. Kordts, S. Wolf, J. Krockenberger, P. Marin-Palomo, C. Weimann, S. Randel, W. Freude, T. J. Kippenberg, and C. Koos, "Ultrafast optical ranging using microresonator soliton frequency combs," *Science* **359**, 887–891 (2018).
6. M.-G. Suh and K. J. Vahala, "Soliton microcomb range measurement," *Science* **359**, 884–887 (2018).
7. S. Zhang, J. M. Silver, X. Shang, L. Del Bino, N. M. Ridler, and P. Del'Haye, "Terahertz wave generation using a soliton microcomb," *Opt. Express* **27**, 35257–35266 (2019).
8. M.-G. Suh, X. Yi, Y.-H. Lai, S. Leifer, I. S. Grudin, G. Vasisht, E. C. Martin, M. P. Fitzgerald, G. Doppmann, J. Wang *et al.*, "Searching for exoplanets using a microresonator astrocomb," *Nat. Photonics* **13**, 25–30 (2019).
9. E. Obrzud, M. Rainer, A. Harutyunyan, M. H. Anderson, J. Liu, M. Geiselmann, B. Chazelas, S. Kundermann, S. Lecomte, M. Cecconi *et al.*, "A microphotonic astrocomb," *Nat. Photonics* **13**, 31 (2019).
10. V. Brasch, M. Geiselmann, T. Herr, G. Lihachev, M. H. P. Pfeiffer, M. L. Gorodetsky, and T. J. Kippenberg, "Photonic chip-based optical frequency comb using soliton cherenkov radiation," *Science* **351**, 357–360 (2016).
11. C. Joshi, J. K. Jang, K. Luke, X. Ji, S. A. Miller, A. Klenner, Y. Okawachi, M. Lipson, and A. L. Gaeta, "Thermally controlled comb generation and soliton modelocking in microresonators," *Opt. Lett.* **41**, 2565–2568 (2016).
12. T. C. Briles, J. R. Stone, T. E. Drake, D. T. Spencer, C. Fredrick, Q. Li, D. Westly, B. R. Ilic, K. Srinivasan, S. A. Diddams, and S. B. Papp, "Interlocking Kerr-microresonator frequency combs for microwave to optical synthesis," *Opt. Lett.* **43**, 2933–2936 (2018).
13. Z. Gong, A. Bruch, M. Shen, X. Guo, H. Jung, L. Fan, X. Liu, L. Zhang, J. Wang, J. Li *et al.*, "High-fidelity cavity soliton generation in crystalline AlN micro-ring resonators," *Opt. letters* **43**, 4366–4369 (2018).
14. Z. Gong, X. Liu, Y. Xu, M. Xu, J. B. Surya, J. Lu, A. Bruch, C. Zou, and H. X. Tang, "Soliton microcomb generation at 2  $\mu\text{m}$  in z-cut lithium niobate microring resonators," *Opt. letters* **44**, 3182–3185 (2019).
15. Y. He, Q.-F. Yang, J. Ling, R. Luo, H. Liang, M. Li, B. Shen, H. Wang, K. Vahala, and Q. Lin, "Self-starting bi-chromatic LiNbO<sub>3</sub> soliton microcomb," *Optica* **6**, 1138–1144 (2019).
16. D. J. Wilson, K. Schneider, S. Hönl, M. Anderson, Y. Baumgartner, L. Czornomaz, T. J. Kippenberg, and P. Seidler, "Integrated gallium phosphide nonlinear photonics," *Nat. Photonics* **14**, 57–62 (2020).
17. L. Chang, W. Xie, H. Shu, Q. Yang, B. Shen, A. Boes, J. D. Peters, W. Jin, S. Liu, G. Moille *et al.*, "Ultra-efficient frequency comb generation in AlGaAs-on-insulator microresonators," *arXiv preprint arXiv:1909.09778* (2019).
18. X. Ji, F. A. S. Barbosa, S. P. Roberts, A. Dutt, J. Cardenas, Y. Okawachi, A. Bryant, A. L. Gaeta, and M. Lipson, "Ultra-low-loss on-chip resonators with sub-milliwatt parametric oscillation threshold," *Optica* **4**, 619–624 (2017).
19. M. H. P. Pfeiffer, J. Liu, A. S. Raja, T. Morais, B. Ghadiani, and T. J. Kippenberg, "Ultra-smooth silicon nitride waveguides based on the Damascene reflow process: fabrication and loss origins," *Optica* **5**, 884–892 (2018).
20. H. El Dirani, L. Youssef, C. Petit-Etienne, S. Kerdiles, P. Grosse, C. Monat, E. Pargon, and C. Sciancalepore, "Ultralow-loss tightly confining Si<sub>3</sub>N<sub>4</sub> waveguides and high-Q microresonators," *Opt. express* **27**, 30726–30740 (2019).

21. B. Stern, X. Ji, Y. Okawachi, A. L. Gaeta, and M. Lipson, "Battery-operated integrated frequency comb generator," *Nature* **562**, 401–405 (2018).
22. A. S. Raja, A. S. Voloshin, H. Guo, S. E. Agafonova, J. Liu, A. S. Gorodnitskiy, M. Karpov, N. G. Pavlov, E. Lucas, R. R. Galiev *et al.*, "Electrically pumped photonic integrated soliton microcomb," *Nat. communications* **10**, 680 (2019).
23. B. Shen, L. Chang, J. Liu, H. Wang, Q.-F. Yang, C. Xiang, R. N. Wang, J. He, T. Liu, W. Xie *et al.*, "Integrated turnkey soliton microcombs operated at CMOS frequencies," arXiv preprint arXiv:1911.02636 (2019).
24. A. S. Voloshin, J. Liu, N. M. Kondratiev, G. V. Lihachev, T. J. Kippenberg, and I. A. Bilenko, "Dynamics of soliton self-injection locking in a photonic chip-based microresonator," arXiv preprint arXiv:1912.11303 (2019).
25. T. C. Briles, J. R. Stone, S. B. Papp, G. Moille, K. Srinivasan, L. Chang, C. Xiang, J. Guo, and J. E. Bowers, "Generation of octave-spanning microresonator solitons with a self injection-locked DFB laser," in *2019 IEEE Avionics and Vehicle Fiber-Optics and Photonics Conference (AVFOP)*, (IEEE, 2019), pp. 1–2.
26. R. Niu, S. Wan, S.-M. Sun, T.-G. Ma, H.-J. Chen, W.-Q. Wang, Z.-Z. Lu, W.-F. Zhang, G.-C. Guo, C.-L. Zou *et al.*, "Repetition rate tuning of soliton in microrod resonators," arXiv preprint arXiv:1809.06490 (2018).
27. S. Zhang, J. M. Silver, L. Del Bino, F. Copie, M. T. Woodley, G. N. Ghalanos, A. Ø. Svela, N. Moroney, and P. Del'Haye, "Sub-milliwatt-level microresonator solitons with extended access range using an auxiliary laser," *Optica* **6**, 206–212 (2019).
28. Z. Lu, W. Wang, W. Zhang, S. T. Chu, B. E. Little, M. Liu, L. Wang, C.-L. Zou, C.-H. Dong, B. Zhao *et al.*, "Deterministic generation and switching of dissipative kerr soliton in a thermally controlled micro-resonator," *AIP Adv.* **9**, 025314 (2019).
29. A. Dutt, C. Joshi, X. Ji, J. Cardenas, Y. Okawachi, K. Luke, A. L. Gaeta, and M. Lipson, "On-chip dual-comb source for spectroscopy," *Sci. advances* **4**, e1701858 (2018).
30. T. Lin, A. Dutt, C. Joshi, C. T. Phare, Y. Okawachi, A. L. Gaeta, M. Lipson *et al.*, "Broadband ultrahigh-resolution chip-scale scanning soliton dual-comb spectroscopy," arXiv preprint arXiv:2001.00869 (2020).
31. E. Lucas, G. Lihachev, R. Bouchand, N. G. Pavlov, A. S. Raja, M. Karpov, M. L. Gorodetsky, and T. J. Kippenberg, "Spatial multiplexing of soliton microcombs," *Nat. Photonics* **12**, 699 (2018).
32. Q.-F. Yang, X. Yi, K. Y. Yang, and K. Vahala, "Counter-propagating solitons in microresonators," *Nat. Photonics* **11**, 560 (2017).
33. M.-G. Suh, Q.-F. Yang, K. Y. Yang, X. Yi, and K. J. Vahala, "Microresonator soliton dual-comb spectroscopy," *Science* **354**, 600–603 (2016).
34. M. Yu, Y. Okawachi, A. G. Griffith, N. Picqué, M. Lipson, and A. L. Gaeta, "Silicon-chip-based mid-infrared dual-comb spectroscopy," *Nat. communications* **9**, 1–6 (2018).
35. C. Bao, M.-G. Suh, and K. Vahala, "Microresonator soliton dual-comb imaging," *Optica* **6**, 1110–1116 (2019).
36. Q.-F. Yang, B. Shen, H. Wang, M. Tran, Z. Zhang, K. Y. Yang, L. Wu, C. Bao, J. Bowers, A. Yariv *et al.*, "Vernier spectrometer using counterpropagating soliton microcombs," *Science* **363**, 965–968 (2019).
37. M. Yu, Y. Okawachi, A. G. Griffith, M. Lipson, and A. L. Gaeta, "Microresonator-based high-resolution gas spectroscopy," *Opt. letters* **42**, 4442–4445 (2017).
38. N. Kuse, T. Tetsumoto, G. Navickaite, M. Geiselmann, and M. E. Fermann, "Continuous scanning of a dissipative Kerr-microresonator soliton comb for broadband, high resolution spectroscopy," arXiv preprint arXiv:1908.07044 (2019).
39. J. Riemensberger, A. Lukashchuk, M. Karpov, W. Weng, E. Lucas, J. Liu, and T. J. Kippenberg, "Massively parallel coherent laser ranging using soliton microcombs," arXiv preprint arXiv:1912.11374 (2019).
40. N. Kuse and M. Fermann, "Frequency-modulated comb LIDAR," *APL Photonics* **4**, 106105 (2019).
41. K. Jung and J. Kim, "All-fibre photonic signal generator for attosecond timing and ultralow-noise microwave," *Sci. reports* **5**, 1–7 (2015).
42. N. Kuse and M. Fermann, "Electro-optic comb based real time ultra-high sensitivity phase noise measurement system for high frequency microwaves," *Sci. reports* **7**, 1–8 (2017).
43. N. Kuse and M. Fermann, "A photonic frequency discriminator based on a two wavelength delayed self-heterodyne interferometer for low phase noise tunable micro/mm wave synthesis," *Sci. reports* **8**, 1–11 (2018).
44. T. E. Drake, J. R. Stone, T. C. Briles, and S. B. Papp, "Thermal decoherence and laser cooling of Kerr microresonator solitons," arXiv preprint arXiv:1903.00431 (2019).
45. G. Huang, E. Lucas, J. Liu, A. S. Raja, G. Lihachev, M. L. Gorodetsky, N. J. Engelsen, and T. J. Kippenberg, "Thermorefractive noise in silicon-nitride microresonators," *Phys. Rev. A* **99**, 061801 (2019).
46. N. Kondratiev and M. Gorodetsky, "Thermorefractive noise in whispering gallery mode microresonators: Analytical results and numerical simulation," *Phys. Lett. A* **382**, 2265–2268 (2018).
47. D. B. Sohn, S. Kim, and G. Bahl, "Time-reversal symmetry breaking with acoustic pumping of nanophotonic circuits," *Nat. Photonics* **12**, 91–97 (2018).
48. S. Hua, J. Wen, X. Jiang, Q. Hua, L. Jiang, and M. Xiao, "Demonstration of a chip-based optical isolator with parametric amplification," *Nat. communications* **7**, 1–6 (2016).
49. D. Huang, P. Pintus, Y. Shoji, P. Morton, T. Mizumoto, and J. E. Bowers, "Integrated broadband Ce: YIG/Si Mach-Zehnder optical isolators with over 100 nm tuning range," *Opt. letters* **42**, 4901–4904 (2017).
50. D. Huang, P. Pintus, and J. E. Bowers, "Towards heterogeneous integration of optical isolators and circulators with lasers on silicon," *Opt. Mater. Express* **8**, 2471–2483 (2018).